



Generation of micro/nano hybrid surface structures on copper by femtosecond pulsed laser irradiation

Ayumi Nakajima¹ · Masaki Omiya² · Jiwang Yan²

Received: 1 January 2022 / Revised: 23 February 2022 / Accepted: 23 February 2022
© The Author(s) 2022

Abstract

The delamination of copper lead frames from epoxy molding compounds (EMC) is a severe problem for microelectronic devices, as it leads to reduced heat dissipation or circuit breakage. The micro/nanoscale surface structuring of copper is a promising method to improve the copper–EMC interfacial adhesion. In this study, the generation of micro/nano hybrid structures on copper surfaces through femtosecond pulsed laser irradiation is proposed to improve interfacial adhesion. The micro/nano hybrid structures were realized by generating nanoscale laser-induced periodic surface structures (LIPSS) on microscale parallel grooves. Several types of hybrid surface structures were generated by changing the laser polarization direction, fluence, and scanning speed. At a specific aspect ratio of microgrooves, a latticed structure was generated on the sides of microgrooves by combining LIPSS formation and direct laser interference patterning. This study provides an efficient method for the micro/nanoscale hybrid surface structure formation for interfacial adhesion improvement between copper and EMC.

Keywords Femtosecond pulsed laser · Copper · Metal surface · LIPSS · Direct laser interference patterning · Micro/nano hybrid structures

1 Introduction

In semiconductor packages, IC chips and copper lead frames are sealed with epoxy molding compounds (EMC) because of the high electrical conductivity of copper and high electrical insulation of EMC [1]. Currently, the demand for semiconductor devices is rising exponentially. However, the delamination of copper lead frames from EMC is a severe problem with semiconductor packages because it leads to reduced heat dissipation or circuit breakage [2]. Delamination is mainly caused by interfacial shear stress due to the difference in thermal expansion between copper and EMC during molding and reflow processes or in the service stage of IC devices [3].

The micro/nanoscale structuring of the metal surface has been proven to improve interfacial adhesion. For example, microscale grooves and nanoscale cone structures have been fabricated by chemical methods, such as etching [4], plating [5], and transcription using a plasma printed punch array [6] for improving interfacial adhesiveness. However, these methods are unsuitable for fabricating micro/nano hybrid structures. In addition, they either need masks or create waste liquids.

This study aims at the generation of micro/nano hybrid structures on copper surfaces through femtosecond pulsed laser irradiation to improve interfacial adhesion between copper and EMC and suppress delamination. Laser processing can fabricate complex and multiscale shapes efficiently without using chemicals. Specifically, laser-induced periodic surface structures (LIPSS) are known to form when ultrashort pulsed laser irradiation is carried out at low laser fluence near the ablation threshold [7–20]. The period of LIPSS depends on the laser wavelength, and the topography of LIPSS can be controlled by using different media in which the sample is soaked [7]. LIPSS have two major categories: those with periods larger than half the laser wavelength are called low spatial frequency LIPSS (LSFL), whereas

✉ Jiwang Yan
yan@mech.keio.ac.jp

¹ School of Integrated Design Engineering, Graduate School of Science and Technology, Keio University, Yokohama 223-8522, Japan

² Department of Mechanical Engineering, School of Science and Technology, Keio University, Yokohama 223-8522, Japan

those with periods smaller than half the laser wavelength are termed high spatial frequency LIPSS (HSFL) [8]. LSFL are thought to be generated by the interaction of the incident laser beam with surface electromagnetic waves (SEW) [9–11], whereas HSFL is generated by higher harmonic generation [12, 13] or self-organization [14], the mechanism of which is still under investigation. In recent years, LIPSS have been applied to control friction, wettability [15–18], and adhesion strength [19], including the mold release ability [20] of metal surfaces. Not only linear LIPSS but also nanodot structures, which are generated by cross scanning the laser beam, have been used to control surface wettability [18].

In this work, micro/nano hybrid surface structuring was attempted by combining LIPSS generation on parallel microgrooves. Several types of hybrid surface structures with different aspect ratios ($AR = \text{depth}/\text{width}$ of microgrooves) and LIPSS arrangements were fabricated. The effects of laser polarization direction and AR of microgrooves on LIPSS formation were investigated. In addition, irradiation was performed by tilting the sample after the microgroove formation, and the effect of the incident angle of the laser beam on the LIPSS formation was investigated. Finally, grid-pattern hybrid structures were fabricated to reduce the structural anisotropy and improve the shear strength of the copper–EMC interface. This study demonstrated an efficient method for hybrid surface structure formation on metals and the possibility of adhesion improvement between metals and polymers.

2 Materials and Methods

Oxygen-free copper plates were used as specimens in the experiment. The plates measured $40 \text{ mm} \times 40 \text{ mm} \times 1 \text{ mm}$, and the surface of the plate was etched before the experiment to remove the oxide layer and contamination. The experimental setup is shown in Fig. 1. The femtosecond pulsed laser oscillator used in the experiment was PHAROS-08-600-PP, manufactured by Light Conversion, Lithuania. The experimental conditions are presented in Table 1. The laser wavelength was 1030 nm, and the repetition frequency was 100 kHz. The spot shape was elliptical, and the major axis was perpendicular to the polarization direction. The energy density of the laser had a Gaussian distribution. All the experiments were carried out in atmospheric conditions at room temperature ($\sim 23 \text{ }^\circ\text{C}$). The laser beam was scanned by a galvanometer scanner in the X and Y directions. The workpiece height in the Z direction was adjusted using a height-adjustable stage.

The micro/nano hybrid structures were fabricated by irradiating the laser in two steps with different parameters, as illustrated in Fig. 2a, b. The first step was forming parallel

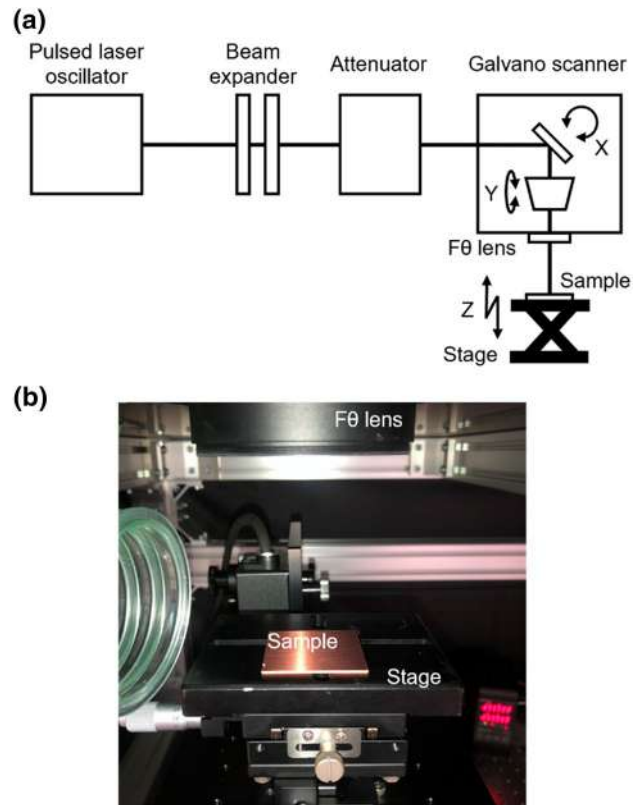


Fig. 1 **a** Diagram of experimental setup, **b** image of sample on the stage

microgrooves at the laser fluence of 2.0, 4.0, 4.5 J/cm^2 and a scanning pitch of 25 and 30 μm on the copper surface (Fig. 2a). The laser fluence and scanning pitch were set so that the top of microgrooves is slightly lower than the unprocessed surface, depending on the spot size and scanning direction. The second step was forming LIPSS on microgrooves with a smaller scanning pitch of 10 μm and a smaller laser fluence of 0.5 J/cm^2 (Fig. 2b). For each step, the laser beam was scanned once.

In the second step, to generate nanoscale latticed structures instead of single-direction LIPSS, a part of the laser

Table 1 Laser irradiation condition

Laser medium	Yb: KGW	
Wavelength λ (nm)	1030	
Spot size (μm)	23×17.5	
Pulse width (fs)	256	
Repetition frequency (kHz)	100	
	Microgroove	LIPSS
Scanning speed V (mm/s)	9.5–80	50
Laser fluence F (J/cm^2)	2.0, 4.0, 4.5	0.2, 0.5, 0.8
Scanning pitch P (μm)	25, 30	10

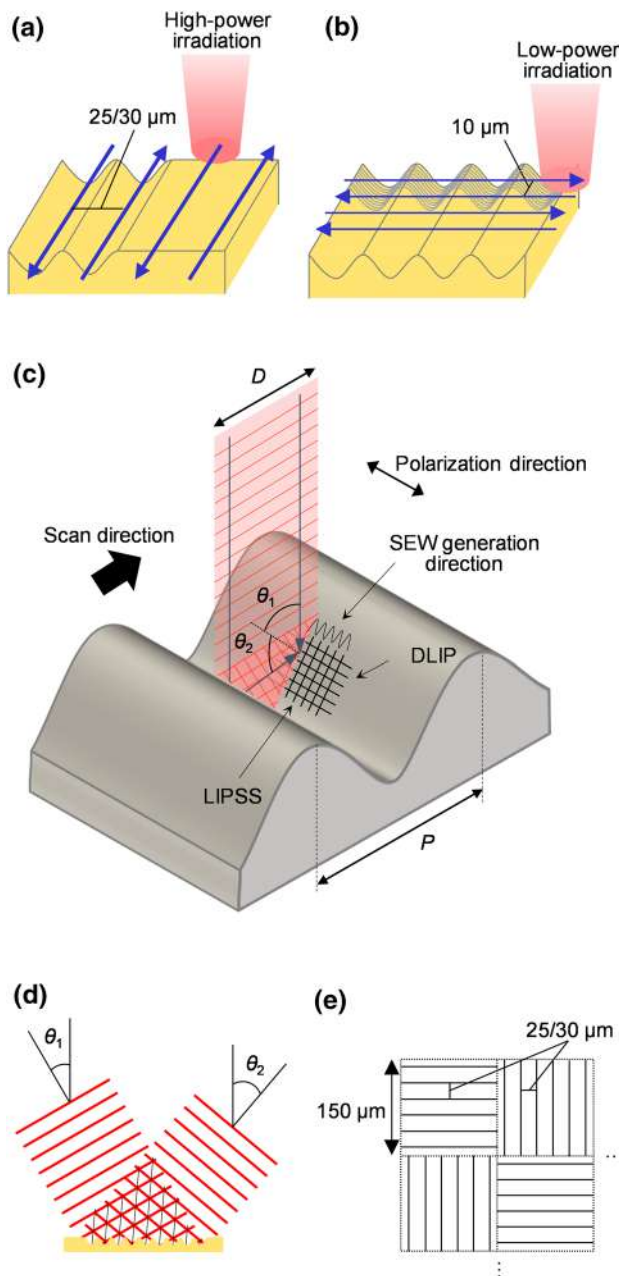


Fig. 2 Schematic of **a** laser irradiation schemes for generating parallel microgrooves, **b** laser irradiation schemes for generating LIPSS on microgrooves, **c** generation mechanism of the latticed structure, **d** DLIP mechanism, **e** laser irradiation schemes for generating grid patterns with hybrid structures

beam was reflected off one side of microgrooves and irradiated on the opposite side, as shown in Fig. 2c. When this reflected laser beam interfered with a directly incoming laser beam on the side surfaces of microgrooves, direct laser interference patterning (DLIP) was realized. The mechanism for DLIP is shown in Fig. 2d. An interference pattern generated by two overlapping laser beams on the surface led to the ablation of the material at the highest intensity areas

producing periodic structures on its surface [21–23]. When the microgroove formation direction and the polarization direction were parallel, the LIPSS direction and the DLIP direction were orthogonal (Fig. 2c). If LIPSS and DLIP overlap perpendicularly, then a latticed structure can be formed [24, 25]. Note that the reflection of the laser depends on the AR, namely, the side surface angles, of the microgrooves formed in the first step. To generate latticed structures, the groove angle may be theoretically predicted or found experimentally. The period of interference pattern Λ is given by the following equation [26].

$$\Lambda = \lambda / (\sin\theta_1 + \sin\theta_2) \quad (1)$$

where θ_1 is the incident beam angle, and θ_2 is the reflected beam angle of the laser, as shown in Fig. 2c and d.

To fabricate grid-pattern hybrid structures, irradiation was performed as shown in Fig. 2e. The size of each grid was 150 μm, in which microgrooves were formed at a scanning pitch of 25 and 30 μm, and the microgrooves in neighboring grids were formed perpendicularly.

After laser irradiation, for the evaluation of microgroove geometry, the cross-sectional profiles were measured by a laser microscope, OLS4100, made by Olympus Corporation, Japan. The surface morphologies of the structured copper plates were observed by a field emission scanning electron microscope (FE-SEM), Inspect F50, made by FEI Company, U.S.

3 Results and Discussion

3.1 Microgroove Formation

The SEM images of microgrooves generated at different laser fluence and scanning speeds are shown in Fig. 3. The surfaces of microgrooves are covered by micrometer-scale debris, which is a result of the redeposition of the ablated material. The groove depth and the amount of debris increased as the scanning speed decreased. The reason is that the number of pulses per unit area increased as the scanning speed decreased and the amount of removed material increased. In addition, LIPSS were vaguely observed at the top of the microgrooves under all conditions. The reason is that the laser fluence at the outer area of a Gaussian beam is lower than that at the beam center. If the laser fluence at the top of a groove is near the ablation threshold, then LIPSS will be locally generated.

3.2 LIPSS Formation

The SEM images of LIPSS generated at different laser fluence are displayed in Fig. 4. At the laser fluence of 0.2 J/

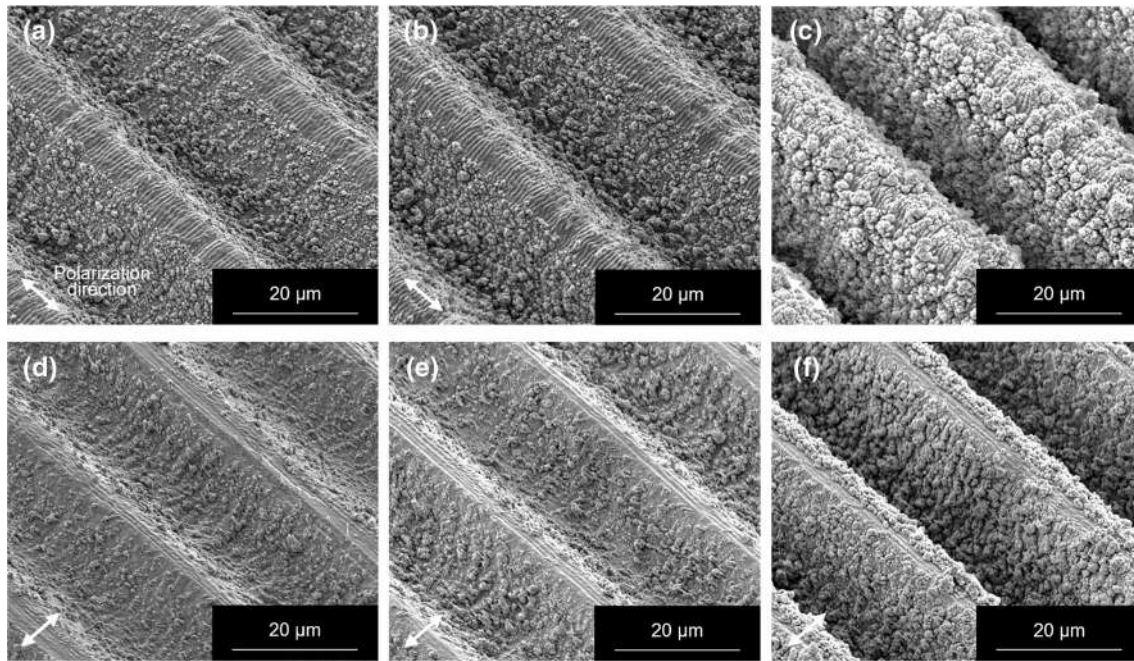


Fig. 3 SEM images of microgrooves with different laser fluence and scanning speeds: **a** 4.0 J/cm², 40 mm/s (AR=0.3), **b** 4.0 J/cm², 30 mm/s (AR=0.4), **c** 4.0 J/cm², 9.5 mm/s (AR=0.7), **d** 4.5 J/cm², 63 mm/s (AR=0.3), **e** 4.5 J/cm², 45 mm/s (AR=0.4), **f** 4.5 J/cm², 22 mm/s (AR=0.7)

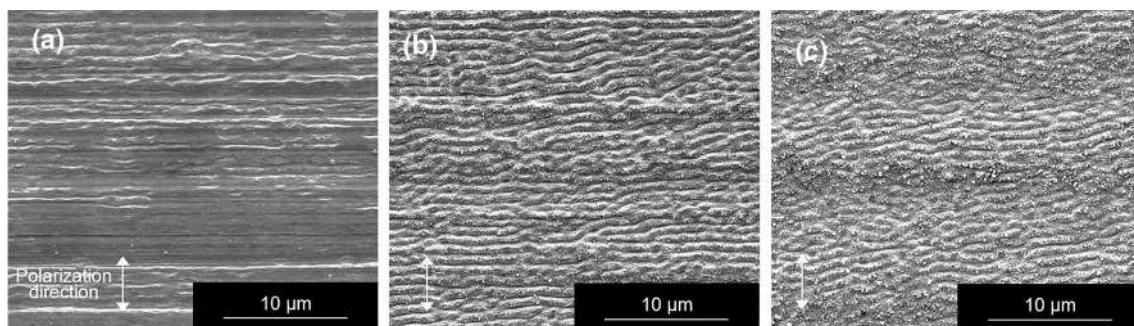


Fig. 4 SEM images of LIPSS with different laser fluence: **a** 0.2 J/cm², **b** 0.5 J/cm², **c** 0.8 J/cm²

cm², almost no LIPSS were generated (Fig. 4a). At the laser fluence of 0.5 J/cm², LIPSS were clearly generated on the whole surface (Fig. 4b). LIPSS were formed perpendicular to the laser polarization direction and had a pitch of 813 ± 34 nm. At the laser fluence of 0.8 J/cm², some areas where LIPSS became unclear were found (Fig. 4c). The reason is that the laser fluence exceeded the ablation threshold, and ablation partially occurred. Therefore, 0.5 J/cm² was selected for the hybrid structure formation in the following experiments.

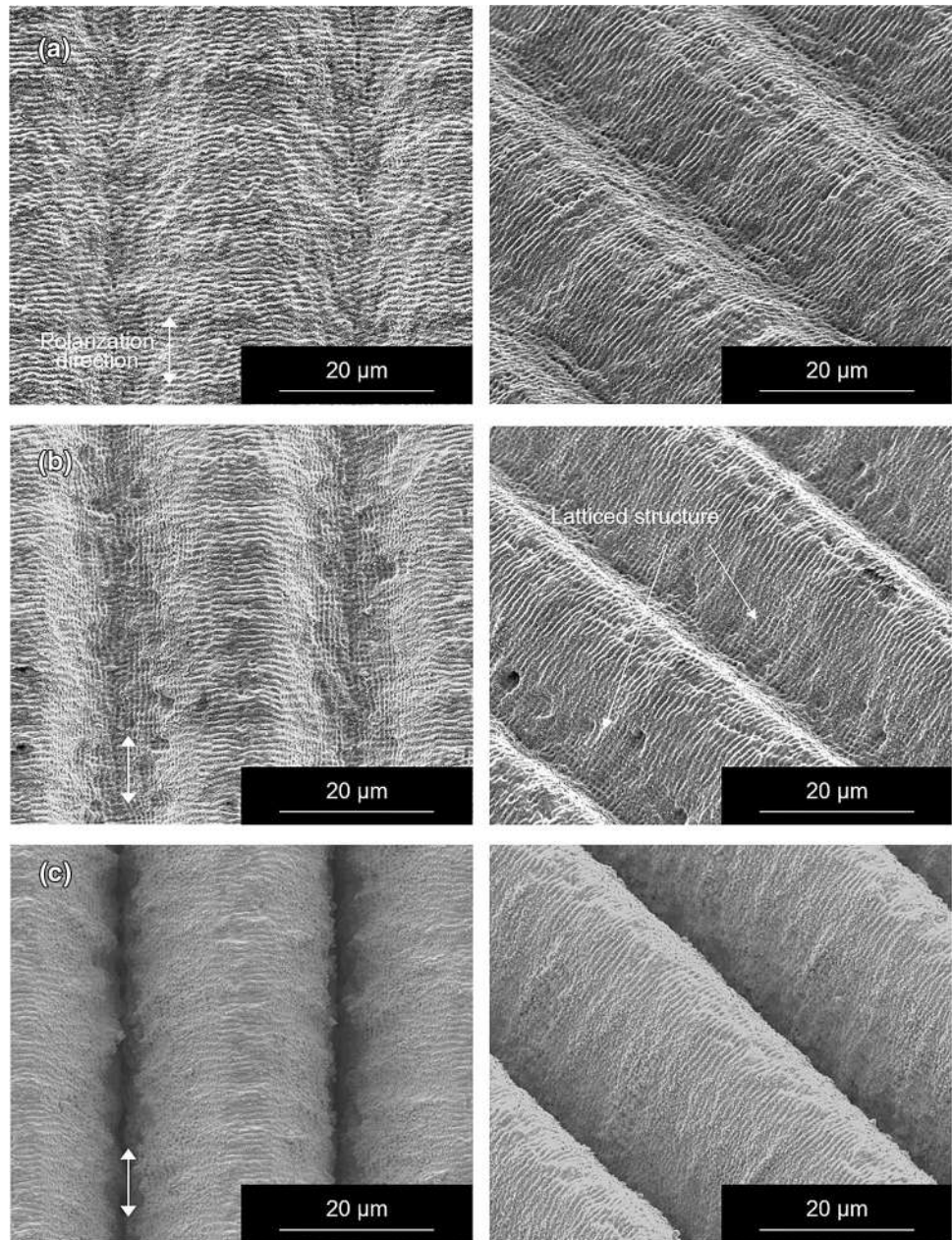
3.3 Hybrid Structure Formation

The SEM images of micro/nano hybrid structures generated at different laser fluence and scanning speeds are displayed

in Fig. 5, where microgrooves are perpendicular to LIPSS, and Fig. 6, where microgrooves are parallel to LIPSS. From these SEM images, it can be observed that the LIPSS formation location depended on the AR of microgrooves and the laser polarization direction. In all hybrid structures, the amount of debris attached to the surface was reduced compared with the microgrooves shown in Fig. 3. The reason may be that the debris generated while creating the microgrooves was removed during LIPSS generation.

When microgrooves and LIPSS were perpendicular to each other (Fig. 5), the period of LIPSS was almost the same as that of LIPSS on the plane (Fig. 4b). When the AR of grooves was small, LIPSS were observed on the whole surface (Fig. 5a); but when the AR was large, LIPSS were not observed on the side surfaces of microgrooves (Fig. 5c). The

Fig. 5 SEM images of hybrid structures with different scanning speeds when microgrooves are perpendicular to LIPSS ($P=30\ \mu\text{m}$): **a** 60 mm/s (AR=0.2), **b** 30 mm/s (AR=0.4), **c** 9.5 mm/s (AR=0.8)

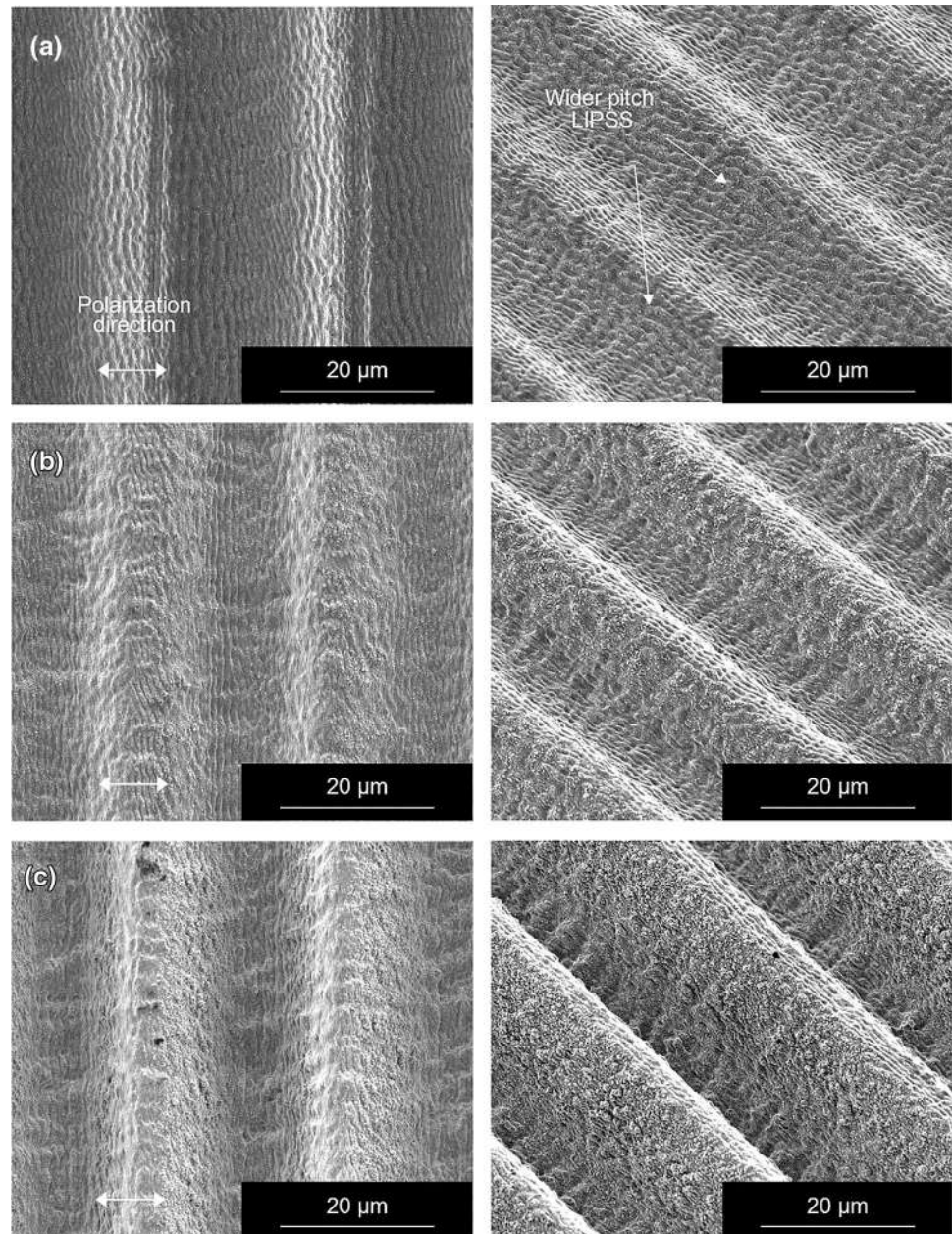


reason for this is that the laser fluence decreases, and LIPSS cannot form when the angle of the side surface is very large.

When AR=0.4, a latticed structure, which may have similar surface functionality to the nanodot structures generated by cross laser scanning [18], was observed on the side surface of microgrooves (Fig. 5b). The latticed structure is a combination of LIPSS and DLIP overlapping perpendicularly, as described in Sect. 2. In Fig. 5b, where $\lambda=1030\ \text{nm}$ and $\theta_1=44^\circ$, $\theta_2=48^\circ$, the period of interference pattern Λ was $716\ \text{nm}$ calculated by Eq. (1). The measured period of the latticed structure was $778 \pm 83\ \text{nm}$, which is almost the same as the calculated value.

When microgrooves and LIPSS were parallel (Fig. 6), clear LIPSS formed at the top and bottom of microgrooves, whereas no LIPSS were observed on the side as the AR of the grooves increased, similar to the case when microgrooves and LIPSS were perpendicular; the reason is that the angle of the microgroove side surface is too large. Another possibility is the effect of the interference pattern occurring parallel to the LIPSS direction. The period of the interference pattern generated on the side of microgrooves by the incident and reflected beams is different from that of LIPSS. Therefore, the generation of an interference pattern may prevent LIPSS formation. When the AR was small, however, LIPSS with a wide period ($1871 \pm 100\ \text{nm}$) formed on the

Fig. 6 SEM images of hybrid structures with different scanning speeds when microgrooves are parallel to LIPSS ($P=25\ \mu\text{m}$): **a** 63 mm/s (AR=0.3), **b** 45 mm/s (AR=0.4), **c** 22 mm/s (AR=0.7)



side of microgrooves (Fig. 6a). The reason is that when the inclination direction and the laser polarization direction are parallel, the electric field strength distribution of the irradiation at an angle of inclination to a surface is wider than that of the irradiation perpendicular to a surface [21].

The cross-sectional profiles of hybrid structures generated at different laser scanning speeds are shown in Fig. 7. Microgrooves were V-shaped only when microgrooves and LIPSS were perpendicular, and the scanning speed was 9.5 mm/s (Fig. 7a). In other cases, the bottom of microgrooves had a round shape.

The change in the depth of hybrid structures obtained at different laser fluence and scanning speeds is illustrated in

Fig. 8. As the laser fluence increased, the depth increased. The depth also increased as the scanning speed decreased. The general trend is the same as that of microgrooves only as described in Sect. 3.1. These results show that the AR of hybrid surface structures can be controlled by changing the polarization direction, fluence, and scanning speed.

3.4 High AR Hybrid Structure Formation

To generate LIPSS on the side of a microgroove with a large AR, after microgroove formation, the sample was tilted by 45° so that the laser beam incident angle became close to 0° , which makes LIPSS formation easy. The SEM image of

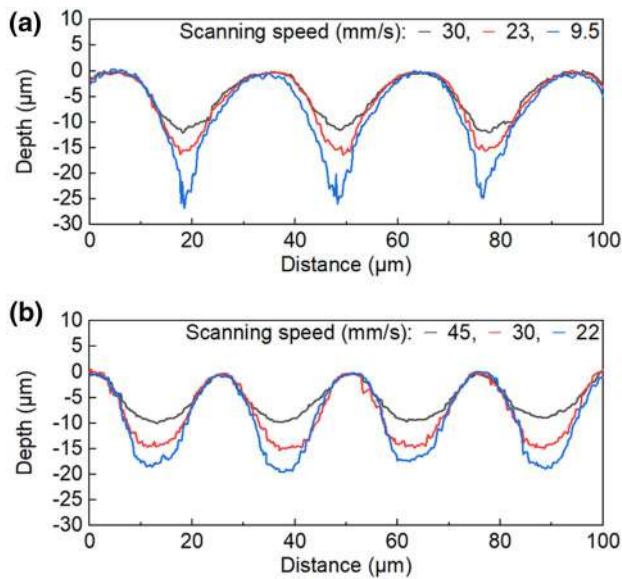


Fig. 7 Cross-sectional profiles of hybrid structures generated at different laser scanning speeds: **a** microgrooves perpendicular to LIPSS ($F=4.0 \text{ J/cm}^2$), **b** microgrooves parallel to LIPSS ($F=4.5 \text{ J/cm}^2$)

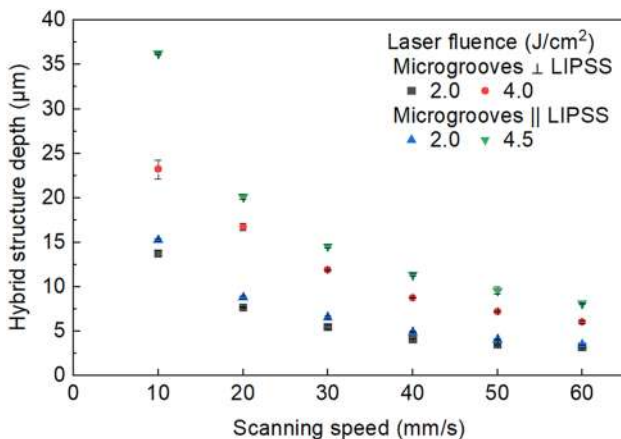


Fig. 8 Hybrid structure depth at different laser fluence and scanning speeds (microgrooves perpendicular to LIPSS: $P=30 \text{ }\mu\text{m}$, microgrooves parallel to LIPSS: $P=25 \text{ }\mu\text{m}$)

the hybrid structure on the tilted samples is shown in Fig. 9. The first step was performed at the laser fluence of 4.5 J/cm^2 , a scanning speed of 30 mm/s , and a scanning pitch of $25 \text{ }\mu\text{m}$ to generate microgrooves. By tilting the sample in the second step, LIPSS were formed clearly on the entire side surfaces of microgrooves. This result demonstrates that forming LIPSS on steep groove side surfaces and groove surfaces that had significant debris deposition after the first step is possible by irradiating the laser perpendicular to the side surface.

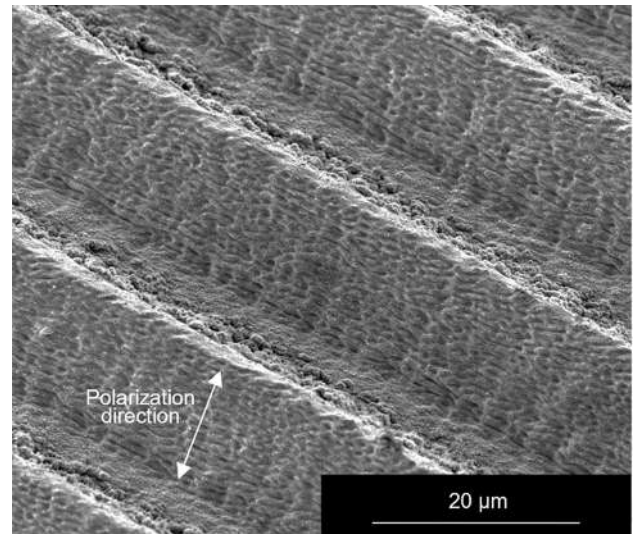


Fig. 9 SEM image of hybrid structure irradiated by tilting the sample in the second step

3.5 Grid-Pattern Hybrid Structure Formation

Finally, grid patterns with hybrid structures were generated using the method shown in Fig. 2e. The SEM images of the grid patterns with hybrid surface structures obtained at different irradiation conditions are presented in Fig. 10. Grid patterns that are composed of two types of hybrid structures, as shown in Fig. 10a, d, were formed. At the laser fluence of 4.5 J/cm^2 , a scanning speed of 80 mm/s , and a scanning pitch of $25 \text{ }\mu\text{m}$, the AR of the microgrooves perpendicular to the polarization direction was 0.24 (Fig. 10b), and that of the microgrooves parallel to the polarization direction was 0.17 (Fig. 10c). Wide-period LIPSS were observed on the side of microgrooves (Fig. 10b). At the laser fluence of 4.0 J/cm^2 , a scanning speed of 30 mm/s , and a scanning pitch of $30 \text{ }\mu\text{m}$, the AR of microgrooves perpendicular to the polarization direction was 0.54 (Fig. 10e), and that of the microgrooves parallel to the polarization direction was 0.38 (Fig. 10f). Latticed structures were observed on the side of microgrooves (Fig. 10f).

The change in the AR of hybrid structures obtained at different scanning speeds and microgroove directions is displayed in Fig. 11. The microgrooves perpendicular to the polarization direction had a higher AR than the microgrooves parallel to the polarization direction. The top of the microgrooves perpendicular to the polarization direction was flat. This is thought to be due to the elliptical nature of the laser spot. When the laser is scanned parallel to the major axis, as the major axis of the elliptical spot is perpendicular to the polarization direction, the pulse overlap increases, resulting in higher material removal. Grid patterns with hybrid structures may provide two-dimensional constraints

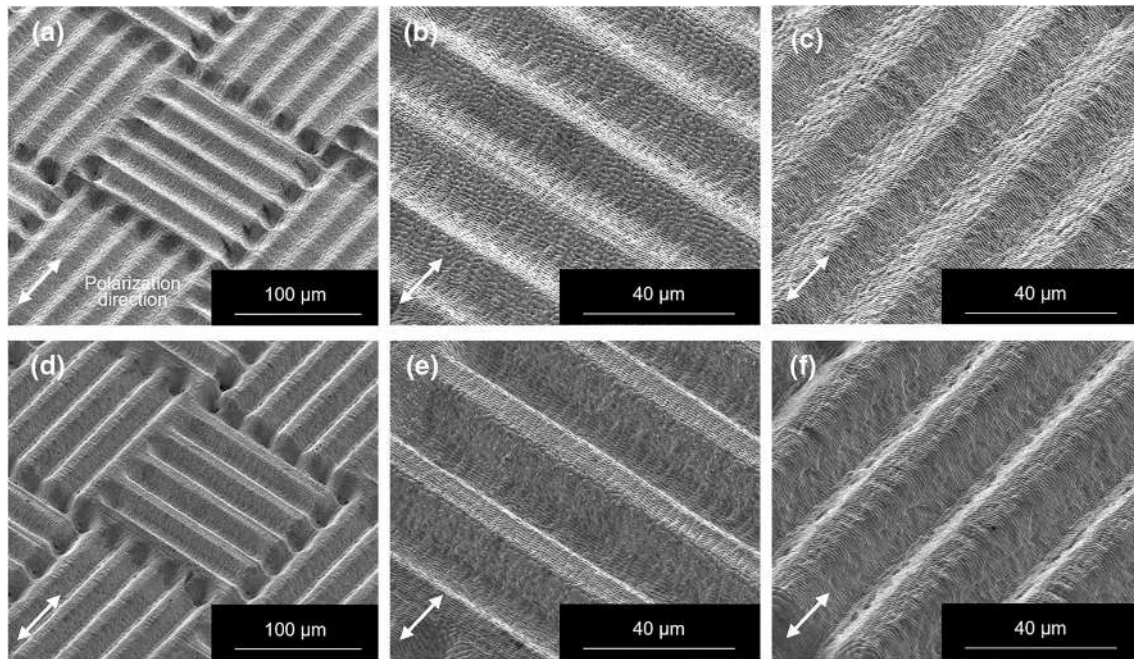


Fig. 10 SEM images of the grid patterns formed by hybrid structures: (a–c) $F=4.5 \text{ J/cm}^2$, $P=25 \text{ } \mu\text{m}$, $V=80 \text{ mm/s}$, (d–f) $F=4.0 \text{ J/cm}^2$, $P=30 \text{ } \mu\text{m}$, $V=30 \text{ mm/s}$

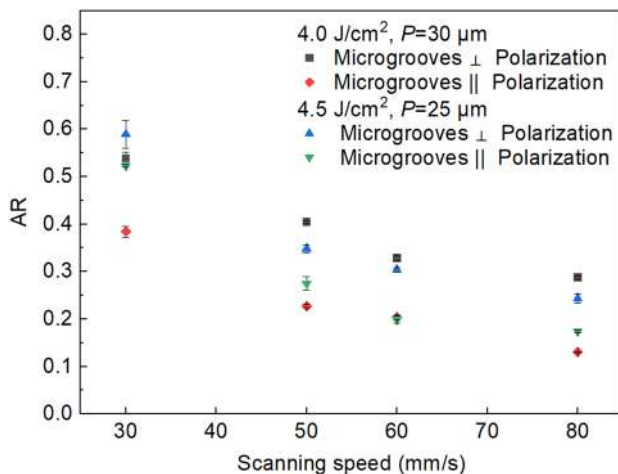


Fig. 11 AR of grid-pattern hybrid structure at different scanning speeds and microgroove directions

of the interfacial flow of EMC against the copper surface, which is expectable to improve the shear strength for IC devices.

4 Conclusions

Femtosecond pulsed laser irradiation was performed on copper to generate micro/nano hybrid surface structures for improving interfacial adhesion between copper and polymers. Hybrid structures combining LIPSS and microgrooves with different AR were formed. At a specific AR, a latticed structure was generated on the side of microgrooves that was formed through the combination of LIPSS and DLIP. Furthermore, grid patterns composed of two types of hybrid structures were fabricated, thereby providing two-dimensional constraints of the interfacial flow of polymer. This study demonstrated a method for hybrid surface structure formation to improve interfacial adhesion and shear strength through femtosecond pulsed laser irradiation. Future works include the optimal hybrid structure design and molding conditions using the hybrid surface structures to maximize adhesion strength.

Conflict of interest There is no conflict of interest.

Open Access This article is licensed under a Creative Commons Attribution 4.0 International License, which permits use, sharing, adaptation, distribution and reproduction in any medium or format, as long as you give appropriate credit to the original author(s) and the source, provide a link to the Creative Commons licence, and indicate if changes were made. The images or other third party material in this article are included in the article's Creative Commons licence, unless indicated otherwise in a credit line to the material. If material is not included in the article's Creative Commons licence and your intended use is not permitted by statutory regulation or exceeds the permitted use, you will

need to obtain permission directly from the copyright holder. To view a copy of this licence, visit <http://creativecommons.org/licenses/by/4.0/>.

References

1. Cho SJ, Paik KW, Kim YG (1997) The effect of the oxidation of Cu-base leadframe on the interface adhesion between Cu metal and epoxy molding compound. *IEEE Trans Compon Packag Manuf Technol Part B* 20(2):167–175. <https://doi.org/10.1109/96.575569>
2. Guo N, Abdul J, Du H, Wong BS (2002) Ultrasonic characterization of the interface between a die attach adhesive and a copper leadframe in IC packaging. *J Adhes Sci Technol* 16(9):1261–1279. <https://doi.org/10.1163/156856102320256882>
3. Chao S-C, Huang W-C, Liu J-H, Song J-M, Shen P-Y, Huang C-L, Hung L-T, Chang C-H (2019) Oxidation characteristics of commercial copper-based lead frame surface and the bonding with epoxy molding compounds. *Microelectron Reliab* 99:161–167. <https://doi.org/10.1016/j.microrel.2019.05.020>
4. Kim WS, Yun IH, Lee JJ, Jung HT (2010) Evaluation of mechanical interlock effect on adhesion strength of polymer–metal interfaces using micro-patterned surface topography. *Int J Adhes Adhes* 30(6):408–417. <https://doi.org/10.1016/j.ijadhadh.2010.05.004>
5. Hang T, Ling HQ, Xiu ZJ, Li M, Mao DL (2007) Study on the adhesion between epoxy molding compound and nanocone-arrayed pd preplated leadframes. *J Electron Mater* 36:1594–1598. <https://doi.org/10.1007/s11664-007-0292-4>
6. Aizawa T, Saito Y, Hasegawa H, Wasa K (2020) Fabrication of optimally micro-textured copper substrates by plasma printing for plastic mold packaging. *Int J Autom Technol* 14(2):200–207. <https://doi.org/10.20965/ijat.2020.p0200>
7. Kobayashi T, Wakabayashi T, Takushima Y, Yan J (2019) Formation behavior of laser-induced periodic surface structures on stainless tool steel in various media. *Precis Eng* 57:244–252. <https://doi.org/10.1016/j.precisioneng.2019.04.012>
8. Bonse J (2020) Quo vadis LIPSS?—Recent and future trends on laser-induced periodic surface structures. *Nanomaterials* 10(10):1950. <https://doi.org/10.3390/nano10101950>
9. Chang C-L, Cheng C-W, Chen J-K (2018) Femtosecond laser-induced periodic surface structures of copper: experimental and modeling comparison. *Appl Surf Sci* 469:904–910. <https://doi.org/10.1016/j.apsusc.2018.11.059>
10. Maragkaki S, Derrien TJ-Y, Levy Y, Bulgakova NM, Ostendorf A, Gurevich EL (2017) Wavelength dependence of picosecond laser-induced periodic surface structures on copper. *Appl Surf Sci* 417:88–92. <https://doi.org/10.1016/j.apsusc.2017.02.068>
11. Garcell EM, Guo C (2018) Polarization-controlled micro-groove arrays induced by femtosecond laser pulses. *J Appl Phys* 123:213103. <https://doi.org/10.1063/1.5028197>
12. Li X-F, Zhang C-Y, Li H, Dai Q-F, Lan S, Tie S-L (2014) Formation of 100-nm periodic structures on a titanium surface by exploiting the oxidation and third harmonic generation induced by femtosecond laser pulses. *Opt Express* 22(23):28086–28099. <https://doi.org/10.1364/OE.22.028086>
13. Trang T, Huynh D, Petit A, Semmar N (2014) Picosecond laser induced periodic surface structure on copper thin films. *Appl Surf Sci* 302:109–113. <https://doi.org/10.1016/j.apsusc.2013.10.172>
14. Reif J, Varlamova O, Varlamov S, Bestehorn M (2011) The role of asymmetric excitation in self-organized nanostructure formation upon femtosecond laser ablation. *Appl Phys A* 104:969–973. <https://doi.org/10.1007/s00339-011-6472-3>
15. Allahyari E, Nivas JJ, Oscurato SL, Salvatore M, Ausanio G, Vecchione A, Fittipaldi R, Maddalena P, Bruzzese R, Amoroso S (2019) Laser surface texturing of copper and variation of the wetting response with the laser pulse fluence. *Appl Surf Sci* 470:817–824. <https://doi.org/10.1016/j.apsusc.2018.11.202>
16. Long J, Fan P, Zhong M, Zhang H, Xie Y, Lin C (2014) Superhydrophobic and colorful copper surfaces fabricated by picosecond laser-induced periodic nanostructures. *Appl Surf Sci* 311:461–467. <https://doi.org/10.1016/j.apsusc.2014.05.090>
17. Aizawa T, Inohara T, Wasa K (2020) Fabrication of superhydrophobic stainless steel nozzles by femtosecond laser micro-/nano-texturing. *Int J Autom Technol* 14(2):159–166
18. Kobayashi T, Yan J (2020) Generating nanodot structures on stainless-steel surfaces by cross scanning of a picosecond pulsed laser. *Nanomanuf Metrol* 3:105–111. <https://doi.org/10.1007/s41871-020-00063-6>
19. Rotella G, Orazi L, Alfano M, Candamano S, Gnilitzky I (2017) Innovative high-speed femtosecond laser nano-patterning for improved adhesive bonding of Ti6Al4V titanium alloy. *CIRP J Manuf Sci Technol* 18:101–106. <https://doi.org/10.1016/j.cirpj.2016.10.003>
20. Kobayashi T, Sera H, Wakabayashi T, Endo H, Takushima Y, Yan J (2018) Surface flattening and nanostructuring of steel by picosecond pulsed laser irradiation. *Nanomanuf Metrol* 1(4):217–224. <https://doi.org/10.1007/s41871-018-0023-x>
21. Takase R, Kodama S, Shimada K, Mescheder H, Winands K, Riepe J, Arntz K, Mizutani M, Kuriyagawa T (2020) Study on the creation of fine periodic structure on V-shaped groove with short-pulsed laser. *Int J Autom Technol* 14(4):601–613. <https://doi.org/10.20965/ijat.2020.p0601>
22. Zheng Y, An Z, Smyrek P, Seifert HJ, Kunze T, Lang V, Lasagni A-F, Pflieger W (2016) Direct laser interference patterning and ultrafast laser-induced micro/nano structuring of current collectors for lithium-ion batteries. *Proc SPIE* 9736, Laser-based Micro- and Nanoprocessing X 97361B. <https://doi.org/10.1117/12.2220111>
23. Fu Y, Soldera M, Wang W, Voisiat B, Lasagni AF (2019) Picosecond laser interference patterning of periodical micro-architectures on metallic molds for hot embossing. *Materials* 12(20):3409. <https://doi.org/10.3390/ma12203409>
24. Alamri S, Fraggelakis F, Kunze T, Krupop B, Mincuzzi G, Kling R, Lasagni AF (2019) On the interplay of DLIP and LIPSS upon ultra-short laser pulse irradiation. *Materials* 12(1018):1–9. <https://doi.org/10.3390/ma12071018>
25. Teutoburg-Weiss S, Sonntag F, Günther K, Lasagni AF (2019) Multiple method micromachining laser platform for fabricating anti-counterfeit elements with multiple-scaled features. *Opt Laser Technol* 115:465–476. <https://doi.org/10.1016/j.optlastec.2019.02.044>
26. Wolfen HV, Abelmann L (2011) Laser interference lithography. In: Hennessy TC (ed) *Lithography: principles, processes and materials*. Nova Science Publishers Inc, New York, pp 133–148